nature structural & molecular biology

A split active site couples cap recognition by Dcp2 to activation

Stephen N Floor[1,2], Brittnee N Jones[2,3], Gail A Hernandez[2,4] & John D Gross[2]

Decapping by Dcp2 is an essential step in 5′-to-3′ mRNA decay. In yeast, decapping requires an open-to-closed transition in Dcp2, though the link between closure and catalysis remains elusive. Here we show using NMR that cap binds conserved residues on both the catalytic and regulatory domains of Dcp2. Lesions in the cap-binding site on the regulatory domain reduce the catalytic step by two orders of magnitude and block the formation of the closed state, whereas Dcp1 enhances the catalytic step by a factor of 10 and promotes closure. We conclude that closure occurs during the rate-limiting catalytic step of decapping, juxtaposing the cap-binding region of each domain to form a composite active site. This work suggests a model for regulation of decapping where coactivators trigger decapping by stabilizing a labile composite active site.

Degradation of mRNA has a crucial role in animal development[1], cell proliferation[2,3], differentiation[4], stress responses[5], the adaptive immune system[6] and transcript quality control[7]. Removal of the 5′-terminal cap structure by the mRNA decapping enzyme Dcp2 is a critical step in numerous 5′-to-3′ decay pathways including bulk 5′-to-3′ decay[8,9], AU-rich element–mediated decay[10,11], nonsense-mediated decay (NMD)[7,12], miRNA-induced decay[13–15] and 3′-uridylation[16–19]. In these pathways, decapping is an irreversible step that exposes the 5′-monophosphate of the RNA body for recognition by conserved 5′-to-3′ exonucleases[20]. Decapping is thus a highly regulated, committed step that sentences an mRNA to destruction.

Regulation of decapping is achieved by a dense network of protein-protein interactions impinging on the decapping enzyme Dcp2 (refs. 7,14, 21–25). Though activation of decapping could be accomplished by targeting the decapping complex to a substrate mRNA, recent work revealed that a conformational change in yeast Dcp2 is used to achieve a switch-like response in activity[26,27]. Crystallographic studies[26,28] indicate that the conserved N-terminal region of Dcp2 has a bilobed architecture containing a regulatory domain, which binds the essential activator Dcp1, and a catalytic domain of the Nudix hydrolase superfamily[26,29,30] (**Fig. 1a**). The cocrystal structure of the *Schizosaccharomyces pombe* Dcp1–Dcp2 complex[26] showed two conformations of Dcp2: one extended and unliganded and the other compact and bound to ATP (**Supplementary Fig. 1a**). NMR and kinetic studies revealed an RNA-binding channel that bisects the regulatory and catalytic domains, suggesting that conformational transitions in Dcp2 control an aspect of substrate recognition and catalysis[26,27].

Four observations suggest that conversion between open and closed states is required for efficient decapping. First, the regulatory domain and Dcp1 together contribute a factor of 1,000 to the catalytic step and ensure correct bond hydrolysis[27,31] but are far removed from the active site in the open form of the Dcp1–Dcp2 complex[26] (**Supplementary Fig. 1a**). Second, the regulatory domain and Dcp1 are essential for decapping in budding yeast[9,28]. Third, the introduction of prolines in the interdomain linker block closure, as detected by small angle X-ray scattering (SAXS), and hinder decapping *in vitro*[26]. Finally, the proline mutations mimic the effect of a Dcp2 knockout on reporter mRNA half-life *in vivo* and cause an accumulation of Dcp2 in P bodies[26]. Enlarged P bodies are also a consequence of lesions in a variety of coactivators of decapping, implicating this conformational change in the activation of decapping *in vivo*[14,22,32–34]. These findings support the notion that conformational changes in Dcp2 constitute a critical, regulated step governing mRNA decapping and transcript stability.

An unresolved question is how closure in Dcp2 is linked to efficient cap hydrolysis. Using the crystal structure of the fission yeast Dcp1–Dcp2 complex as a guide[26], we show that mutation of conserved residues of the regulatory domain retards the catalytic step and blocks closure. Unexpectedly, a surface of the regulatory domain specifically interacts with m^7G, whereas the catalytic domain binds multiple nucleotides using different surfaces. We show that Dcp1 enhances the catalytic step by a factor of 10 *in vitro*, likely by stabilizing the closed conformation[26]. We propose a composite active-site model of decapping where the regulatory domain makes specific interactions with the cap, positioning it for pyrophosphatase chemistry catalyzed by the Nudix domain.

RESULTS

Mutations on the regulatory domain retard the catalytic step

To determine how closure contributes to catalysis, we sought to disrupt the closed crystal form (PDB 2QKM[26]) and test for kinetic defects. We selected sites along the 31–52 helix of *S. pombe* Dcp2 involved in the closed-form interdomain interface, mutated them to alanine and

[1]Graduate Group in Biophysics, University of California, San Francisco, California, USA. [2]Department of Pharmaceutical Chemistry, University of California, San Francisco, California, USA. [3]Program in Chemistry and Chemical Biology, University of California, San Francisco, California, USA. [4]Present address: Department of Chemistry, University of Chicago, Chicago, Illinois, USA. Correspondence should be addressed to J.D.G. (jdgross@cgl.ucsf.edu).

Received 5 February; accepted 18 June; published online 15 August 2010; doi:10.1038/nsmb.1879

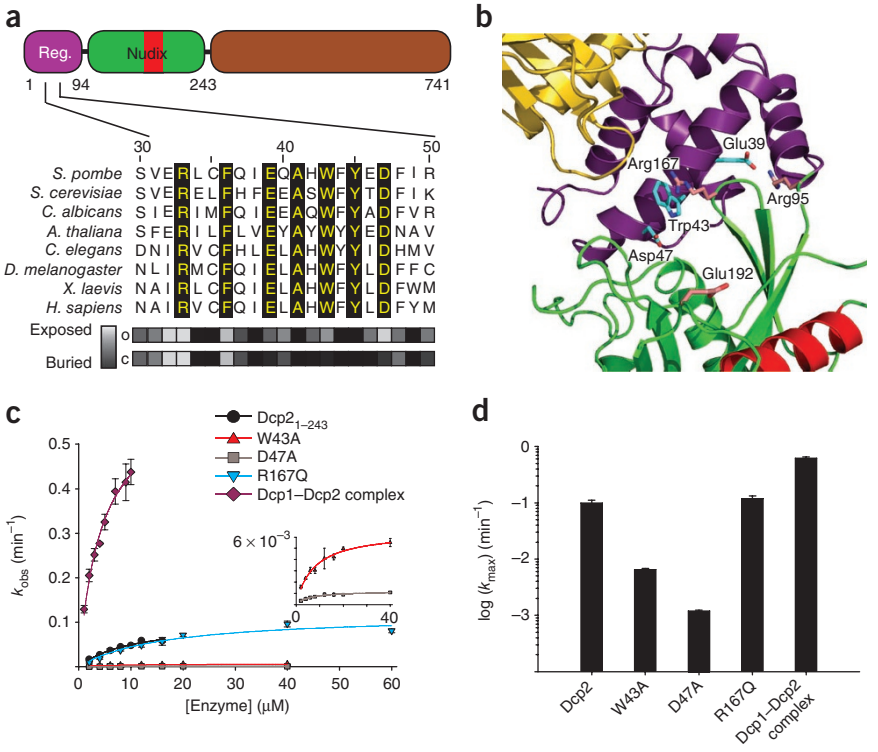

Figure 1 Mutants along the interdomain interface in the closed crystal form attenuate the catalytic step of decapping. (**a**) Dcp2 consists of an N-terminal regulatory domain (1–94, purple), a catalytic domain of the Nudix superfamily (95–243, green with the Nudix motif in red) and a large, nonconserved C-terminal region of unknown function (244–741, brown). A sequence alignment is provided for residues 30–50 of Dcp2, with absolutely conserved residues highlighted in yellow. For residues 30–50, the solvent-accessible surface area (SASA) is shown on a relative scale from buried to exposed in both the open (o) and closed (c) crystal forms (for details, see Online Methods). (**b**) The interface between the regulatory domain (purple) and the catalytic domain (green) in the closed, ATP-bound crystal structure is shown with sites of mutation highlighted (PDB 2QKM[26]). Gold, Dcp1; red, catalytic Nudix helix of Dcp2. (**c**) Observed rate constants for decapping assays of various constructs as marked. Solid lines are fitted to a rate equation appropriate for single-turnover kinetics, where enzyme is in excess of substrate[35] (see **Supplementary Note**). Error bars, s.e.m. for the rate measured in two or more independent experiments. (**d**) The rate of the catalytic step (k_{max}) is plotted on a log scale for selected interface mutants; error is s.e.m.

performed kinetic analyses[27,35] (**Fig. 1a**,**b**). Because of their superior solubility, we used decapping proteins from *S. pombe* and cite residue numbers accordingly. Candidate interactions that could stabilize the closed form include a salt bridge between Glu39 and Arg95, an apparent cation-π interaction between Trp43 and Arg167 and a contact between Asp47 and the backbone of Tyr220 (ref. 26) (**Fig. 1b**). We narrowed our focus to Trp43 and Asp47, as a previous alanine scanning study indicated that mutation of these conserved residues resulted in the strongest decapping defects observed on a reporter mRNA in yeast[28]. Alanine substitution at positions 43 and 47 attenuated decapping activity in our single-turnover kinetic assay, consistent with previous *in vitro* endpoint assays[28] (**Fig. 1c**). Mutation at Trp43 or Asp47 reduces the catalytic step (k_{max}) by a factor of 20 or 100, respectively, whereas K_M was nearly unchanged (**Fig. 1d** and **Table 1**). Given the location of Trp43 and Asp47, the attenuation of the catalytic step is likely achieved by destabilizing the active species.

Mutations on the regulatory domain block closure

The kinetic analyses above cannot distinguish between defects in conformational changes or chemistry, as both are proposed to occur in the catalytic step. As such, we turned to SAXS to directly test the effect of the mutants on conformational changes in Dcp2. It was previously established that a compaction of the Dcp1–Dcp2 complex occurs in the presence of ATP or substrate analogs[26]. We reproduced these data on a C-terminal deletion construct (1–243) that is more amenable to solution NMR spectroscopy but has the same activity *in vitro* (**Fig. 2a** and **Supplementary Fig. 1b**). The distance distribution function *P(r)* reveals a compaction in the presence of the cap analog m^{7}GpppA, which is small but reproducible ($n = 3$) (**Fig. 2b**). In response to nucleotide addition, the radius of gyration R_g shrinks from 31.4 ± 1 Å to 28.1 ± 1 Å, and the maximum interatomic distance D_{max} is reduced from 135 ± 10 Å to 105 ± 10 Å in the unbound and liganded experiments, respectively. The region of *P(r)*, which changes upon ligand addition (60–100 Å), is similar to the region that changes between the computed *P(r)* curves from the open and closed crystal forms (**Supplementary Fig. 1c–e**). Differences between the apo solution scattering and open crystal form (**Supplementary Fig. 1c**) or between the liganded solution scattering and closed crystal form (**Supplementary Fig. 1d**) likely result from averaging due to a heterogeneous population, potentially including a mixture of the open and closed crystal forms or alternative states.

In contrast to the compaction observed in wild-type (WT) Dcp1–Dcp2, SAXS analysis of the Dcp1–Dcp2 W43A mutation shows no change in R_g or the distance distribution function between 60 and 100 Å upon addition of cap analog (**Fig. 2c**). The D47A mutation did not have a visible effect on the SAXS distance distribution function (data not shown). We therefore conclude that mutation at Trp43 alters the conformational states accessible to Dcp2 and that Asp47 may affect either the chemical or conformational step, or both.

Table 1 Kinetic rate constants for Dcp2 *in vitro*

Protein	K_M (μM)[a]	k_{max} (min^{-1})[a]	k_{max}/K_M (min^{-1}/μM)	k_{max}/K_M (mut/WT)
WT Dcp2$_{1–243}$	10.1 ± 2.30	$9.98 \times 10^{-2} \pm 1.16 \times 10^{-2}$	9.88×10^{-3}	1
W43A	7.42 ± 0.938	$6.52 \times 10^{-3} \pm 3.00 \times 10^{-4}$	8.78×10^{-4}	0.089
D47A	5.43 ± 0.737	$1.19 \times 10^{-3} \pm 5.20 \times 10^{-5}$	2.19×10^{-4}	0.022
R167Q	16.2 ± 4.75	$1.18 \times 10^{-1} \pm 1.41 \times 10^{-2}$	7.28×10^{-3}	0.74
Dcp2$_{1–243}$ + Dcp1	4.33 ± 0.487	$6.19 \times 10^{-1} \pm 3.01 \times 10^{-2}$	1.43×10^{-1}	14

[a]Error is s.e.m.

Dcp1 enhances the catalytic step

Previous kinetic studies of *Saccharomyces cerevisiae* proteins indicated that Dcp1 and the regulatory domain of Dcp2 contribute a

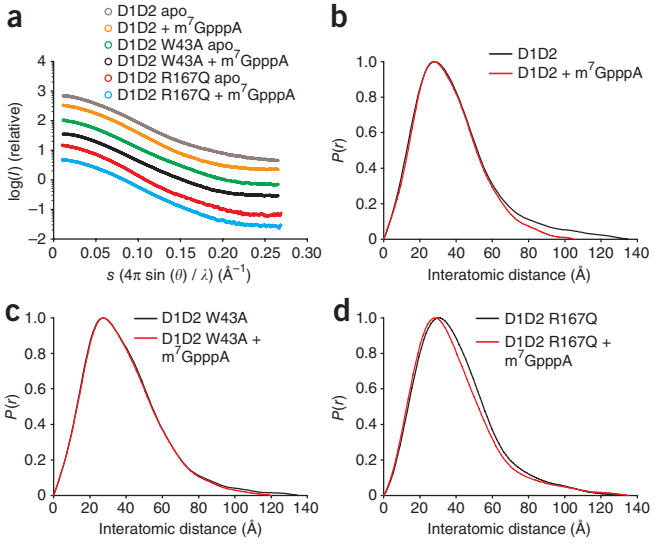

Figure 2 Some interface mutants block conversion to the closed form measured by SAXS. (**a**) Experimental SAXS curves for the WT Dcp1–Dcp2 complex (D1D2) and mutants. Shown is the momentum transfer *s*, where 2θ is the scattering angle and λ is the X-ray wavelength. Scattering curves are artificially displaced along the ordinate for clarity. (**b**) Plotted is the distance distribution function *P(r)* versus interatomic separation (*r*) for the WT decapping complex. Black, unliganded D1D2; red, curve in the presence of 10 mM m^7GpppA. A compaction is evident by the reduced probability between 60 Å and 100 Å in nucleotide bound (red) versus apo (black). (**c**) The observed compaction is blocked upon W43A mutation of Dcp2. (**d**) The R167Q mutation of Dcp2 still closes upon addition of nucleotide.

factor of 1,000 to the catalytic step of decapping[27]. Unlike the decapping proteins from *S. cerevisiae*, Dcp1 and Dcp2 from *S. pombe* can be expressed in *Escherichia coli* and purified separately[28], allowing us to directly quantify the catalytic enhancement by Dcp1. Dcp1 stimulates the catalytic step (k_{max}) by 10 times, with only a small change in K_M (**Fig. 1c**,**d** and **Table 1**). We only detected nucleotide-driven closure of *S. pombe* Dcp2 by SAXS in the presence of Dcp1, suggesting that it may affect the conformational equilibrium that could manifest in this rate enhancement[26]. Therefore, the enhancement previously measured[27] consists of a factor of 10 from Dcp1 and 100 from the regulatory domain.

The ATP-bound and active forms may be distinct

The rationale for mutation at Trp43 is its apparent cation-π interaction with Arg167 in the ATP-bound closed conformation[26] (**Fig. 1b**). However, mutation of the nonconserved residue Arg167 to glutamine (**Fig. 1c**,**d**) or alanine has no effect on decapping *in vitro*[26]. Consistent with the kinetic data, R167Q transitions into a compact state upon addition of m^7GpppA (**Fig. 2d**). Differences in the R167Q distance distribution functions (**Fig. 2d**) compared to WT (**Fig. 2b**) are largely due to a difference in unliganded R167Q versus unliganded WT Dcp2. Therefore, Trp43 retards the catalytic step by blocking closure independently of Arg167, and conversely, Arg167 is not involved in stabilizing the active conformation of Dcp2. This suggests that the interdomain interface in the active form may be different than that observed in the ATP-bound crystal structure[26].

The regulatory domain harbors a binding site for cap

We previously determined that substrate RNA is bound by the catalytic domain of *S. cerevisiae* Dcp2 and that N7-methyl cap is specifically recognized during the catalytic step[27]. However, it was not possible to address the structural foundation of this effect due to the limited solubility of budding yeast Dcp2 constructs[27]. Because closure is promoted by nucleotide, we reasoned that formation of a compact, active form was likely driven by direct contacts between the two domains and cap. Therefore, we used a fragment-based strategy to test the ability of each domain of *S. pombe* Dcp2 to bind m^7GDP product and a panel of nucleotides by NMR, starting with the regulatory domain (residues 1–94, **Fig. 1a**). Unexpectedly, we found that the regulatory domain has an evolutionarily conserved binding site for m^7GDP (**Fig. 3a**,**b**). We detected strong chemical-shift perturbations at both the Trp43 and Asp47 positions and the surrounding 31–52 helix (**Fig. 3c**,**d** and **Supplementary Fig. 2a**). The HSQC titrations were fitted well by a two-state binding model that is used throughout to calculate dissociation constants, consistent with the colinearity of the chemical-shift perturbations (**Fig. 3c**,**d** and **Supplementary Fig. 2b**). Fitting of HSQC titrations for the Trp43 indole and Asp47 backbone amide yields a K_d for m^7GDP of roughly 12 mM, suggesting a concerted binding process (**Supplementary Table 1**). Direct binding of cap by the regulatory domain suggests how substrate binding may stimulate closure.

We next tested the specificity of this binding site by titrating different nucleotides against the domain, and we found that GDP

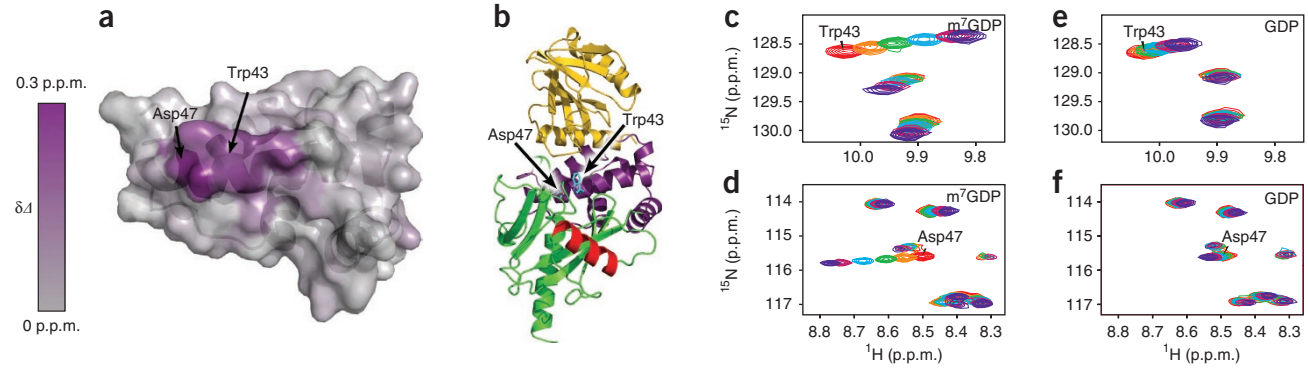

Figure 3 The regulatory domain has a specific binding site for m^7G. (**a**) The regulatory domain colored by chemical-shift perturbation upon addition of 30 mM m^7GDP. Sites of mutation and quantitative analysis, Trp43 and Asp47, are indicated. (**b**) A view of the Dcp1–Dcp2 complex aligned with the isolated regulatory domain (PDB 2QKM[26]). Colors are as in **Figure 1b**. (**c**,**d**) HSQC spectral overlay of the Trp43 indole region (**c**) or the Asp47 backbone (**d**) while being titrated by m^7GDP. Concentrations of nucleotide shown are 0 mM (red), 2.5 mM (orange), 5 mM (green), 10 mM (cyan), 20 mM (pink) and 30 mM (purple). (**e**,**f**) HSQC spectral overlay of the Trp43 indole region (**e**) or the Asp47 backbone (**f**) over the same concentration range of GDP.

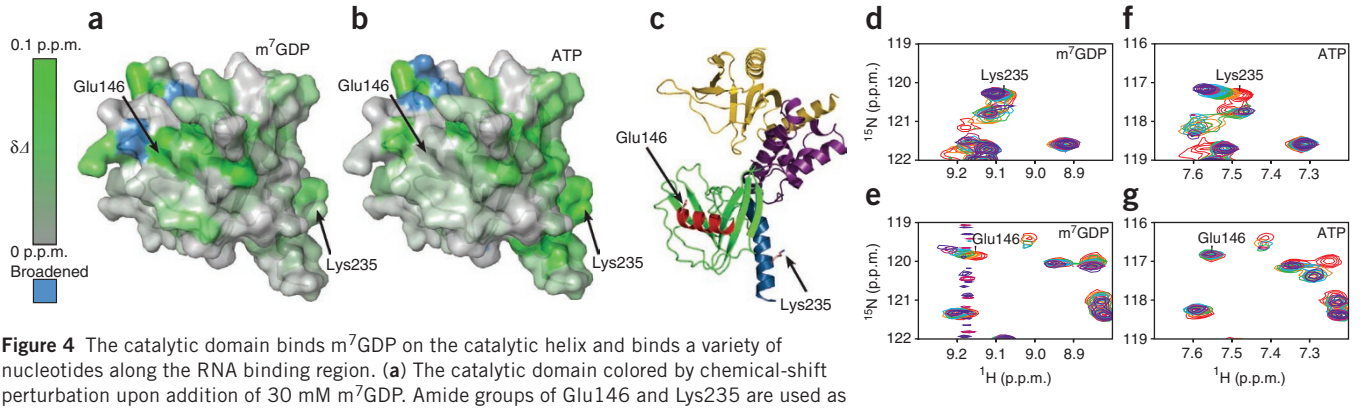

Figure 4 The catalytic domain binds m^7GDP on the catalytic helix and binds a variety of nucleotides along the RNA binding region. (**a**) The catalytic domain colored by chemical-shift perturbation upon addition of 30 mM m^7GDP. Amide groups of Glu146 and Lys235 are used as representatives for binding to the catalytic helix and the RNA binding region, respectively. Blue indicates resonances that were broadened beyond detection upon addition of nucleotide. (**b**) The catalytic domain colored by chemical-shift perturbation upon addition of 30 mM ATP on the same scale as **a**. (**c**) A view of the Dcp1–Dcp2 complex aligned with the isolated catalytic domain (PDB 2QKM[26]). Colors are as in **Figure 1b**, with the RNA binding region highlighted in blue. (**d**,**e**) HSQC spectral overlay of Lys235 (**d**) or Glu146 (**e**) while being titrated by m^7GDP. Colors are the same as in **Figure 3**. The noise in the m^7GDP Glu146 region results from incomplete suppression of uncoupled magnetization of nucleotide due to the phase cycling used in the FHSQC sequence and did not affect the interpretation of the data or the fit[46]. (**f**,**g**) HSQC spectral overlay of Lys235 (**f**) or Glu146 (**g**) while being titrated with ATP.

bound weakly to the same site (**Fig. 3e**,**f** and **Supplementary Fig. 2c**) and that neither ATP nor other nucleoside diphosphates bound to this site (**Supplementary Fig. 2d** and data not shown). Quantification of the data shows that the GDP K_d is weaker at ~40 mM (**Supplementary Fig. 2e** and **Supplementary Table 1**). Therefore, this site is specific for the guanine base and has enhanced affinity for the N7-methylated form. Critically, mutation of Trp43 to alanine blocks m^7GDP binding, directly implicating Trp43 in the binding process and suggesting that mutation at Trp43 blocks closure by decoupling the regulatory domain from cap recognition (**Supplementary Fig. 2f**).

As m^7GDP is a product of the decapping reaction, it is possible that its binding to the regulatory domain is different than that of the substrate RNA cap. Therefore, we tested binding of the cap analog m^7GpppA and found that it binds the same surface with nearly identical affinity to that of m^7GDP (**Supplementary Fig. 3** and **Supplementary Table 1**). In contrast, ApppA does not bind the regulatory domain (**Supplementary Fig. 4**). These data indicate that the addition of adenine, which would correspond to the first transcribed nucleotide of the mRNA, does not affect the recognition of m^7G by the regulatory domain.

The catalytic domain binds m^7G and ATP at different sites

If there is a ligand-dependent coupling between the two domains, then the catalytic domain should also bind nucleotide. To test this we again used HSQC titration to assess the nucleotide binding ability of the catalytic domain (residues 95–243 of *S. pombe* Dcp2, **Fig. 1a**). Three regions were perturbed upon addition of nucleotide: the convex dorsal surface (residues 224–243), the ATP-binding pocket in the crystal structure of *S. pombe* Dcp1–Dcp2 (residues 116–122, 129 and 220–222 (ref. 26)) and the catalytic helix (residues 136–148). There is a clear difference in the binding profile of m^7GDP and ATP for these regions (shifts depicted on PDB 2QKM[26], **Fig. 4** and **Supplementary Fig. 5**). The dorsal surface was perturbed upon addition of either ATP or m^7GDP (**Fig. 4d**,**f**). This region is positively charged and was shown to bind the RNA body nonspecifically, consistent with its lack of specificity for nucleotide[27]. Similarly, the ATP-binding pocket of the protein is the canonical substrate binding region in Nudix hydrolases[29] and binds both nucleotides tested. We directly tested the contribution of the γ phosphate on ATP by titrating ADP against the catalytic domain and found results similar to those with ATP but with reduced affinity, consistent with the interaction being driven by electrostatics (**Supplementary Fig. 6** and **Supplementary Table 1**). Notably, there is agreement between the ATP binding site in the closed crystal state[26], the RNA-binding channel determined in a previous study[27] and the regions detected by NMR chemical-shift perturbation in this work.

In contrast to the dorsal surface and the ATP binding pocket, the catalytic helix was selectively perturbed upon addition of m^7GDP but not ADP or ATP (**Fig. 4a**,**b**,**e**,**g** and **Supplementary Fig. 6**). Binding of m^7GDP also caused perturbations around the catalytically essential residue Glu192, pointing at a potential interaction between Glu192 and cap or remodeling of the 161–194 loop that is not detected by NMR in the presence of ATP or ADP (**Figs. 1b** and **4a** and **Supplementary Fig. 5a**) The previously determined location of the 5′-phosphate of the RNA body places the cap close to the catalytic helix, which is consistent with the perturbations we see upon addition of m^7GDP. Moreover, we previously showed that residues in the catalytic helix are perturbed by nonhydrolyzable capped RNA but not 5′-hydroxyl RNA[27]. In conclusion, the catalytic helix has a specific binding site for cap, whereas the dorsal surface binds the RNA body.

We selected two probes for quantification: the conserved Nudix motif residue Glu146 on the catalytic helix and Lys235 on the RNA-binding region. ATP binds the RNA-binding helix (Lys235) with a K_d of ~5 mM but not does not detectably bind the catalytic helix (**Supplementary Fig. 5d** and **Supplementary Table 1**). In contrast, m^7GDP binds to the catalytic helix (Glu146) with a K_d of 12 mM but only weakly perturbs the RNA binding helix (**Supplementary Fig. 5c** and **Supplementary Table 1**). Unexpectedly, the affinity of m^7GDP for the catalytic helix and regulatory domain are nearly identical, hinting at a concerted binding process in the two-domain protein. These results suggest that Dcp2 has a composite active site that forms as a result of closure, with cap-specific contacts formed by the regulatory and catalytic domains.

DISCUSSION

In this work, we uncovered the role of conformational changes in the catalytic mechanism of Dcp2 and the driving force for conversion into the active form. Dcp1 and the regulatory domain contribute factors of 10 and 100 to the catalytic step, respectively, by modulating conformational states of Dcp2 (**Fig. 1**). The regulatory domain enhances

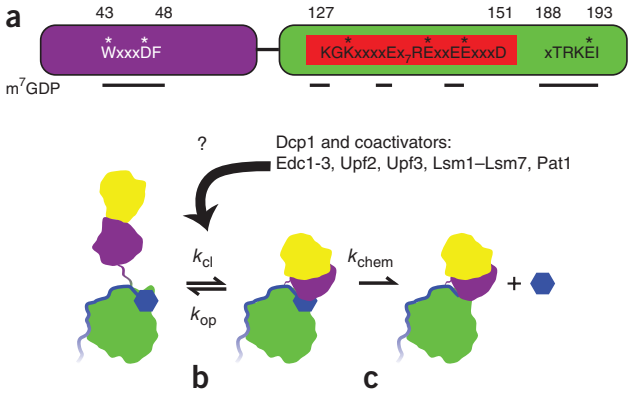

Figure 5 Decapping by Dcp2 proceeds by the formation of a composite active site involving both the regulatory and catalytic domains. (**a**) Regions on the regulatory and catalytic domains that are perturbed by m^7GDP or m^7GpppA cap analog but not other nucleotides are indicated with a bar. Residue boundaries of the regions are indicated above the diagram. Conserved residues are shown in capital letters and those that have strong effects on decapping *in vivo* when mutated are marked with an asterisk (*). Highlighted in red is the conserved Nudix motif, consisting of $GX_5EX_7REUXEEXGU$, with X representing any residue and U representing isoleucine, leucine or valine. (**b**) Isomerization into the active form requires direct interactions of both domains with cap. Colors are as in **Figure 1b**, with RNA indicated in blue with a hexagon cap. k_{op}, rate of opening; k_{cl}, rate of closing. (**c**) Once the active state is formed, decapping proceeds efficiently using a composite active site with cap sandwiched between the two domains. k_{chem}, rate of the chemical step.

the catalytic step by specifically binding m^7G on a conserved surface surrounding Trp43 and Asp47 (**Figs. 1** and **3** and **Supplementary Fig. 3**). Lesions in the cap-binding site block closure and retard the catalytic step by up to two orders of magnitude (**Figs. 1** and **2**), consistent with the severe decapping defect *in vivo* upon mutation of Trp43 or Asp47 (ref. 28). These findings indicate that conversion to the active form of Dcp2 is driven through specific cap recognition by the regulatory domain and suggest that the active form harbors a composite active site with both domains sandwiching the cap.

Nudix family members contain a conserved catalytic motif with additional insertions or domains conferring substrate specificity[29,36]. Dcp2 conforms to this paradigm, with the catalytic domain performing chemistry and the regulatory domain providing specificity by accelerating catalysis on N7-methyl–capped substrates. Notably, the addition of m^7GDP perturbs residues on the conserved, catalytic Nudix helix, whereas ATP and ADP do not (**Figs. 4** and **5a**). The regulatory domain may contribute to catalysis by positioning substrate, as it is required to hydrolyze the correct phosphate bond[31]. High-resolution structural studies of Dcp2 in complex with substrate will be required to confirm this prediction.

The cap-bound conformation is different than the ATP-bound closed form for four reasons. First, the cap-binding residues Trp43 and Asp47 of the regulatory domain are buried in the closed structure and do not contact ATP[26] (**Fig. 1a**,**b**). Second, the regulatory domain and catalytic helix both bind m^7GDP by NMR but are separated by ~20 Å in the closed crystal structure[26] (**Fig. 5a** and **Supplementary Fig. 1a**). Third, Trp43 forms an apparent cation-π interaction with Arg167 of the catalytic domain, but mutating Arg167 to glutamine or alanine does not affect closure or decapping *in vitro*[26] (**Fig. 1b–d**). Fourth, in the closed, ATP-bound form of Dcp1–Dcp2, nonconserved residues 244–266 of the catalytic domain fold into a helix that interacts with the regulatory domain, yet deletion of these residues has no effect on decapping or closure *in vitro*[26,28] (**Supplementary Fig. 1b**). It is unclear whether the ATP-bound form represents an on- or off-pathway state, but it is accessible in solution, as ATP causes closure[26]. Dcp2 may assume different conformations from specific or nonspecific interactions with substrate, as described for other nucleic acid–binding proteins[37,38]. Given the composite active site suggested here and the previous crystal structure with open and closed conformations[26], we conclude that the native energy landscape of Dcp2 is rugged with multiple accessible states depending on the ligand.

Activation of decapping by closure was postulated to be a late step in 5′-to-3′ decay that is promoted by coactivators[26,33]. Dcp2 with proline-hinge mutants blocking closure still localizes to P bodies, but the decay of messages is blocked[26]. Large P bodies containing Dcp2 and decay substrates are a hallmark of stalled decay complexes or overwhelmed decay machinery and are observed in coactivator mutants[22,32,34]. The proline-hinge mutants also cause a dramatic defect in bulk mRNA decay both *in vitro* and *in vivo*[26]. The conformational change detailed here is likely part of this late, regulated step, as mutation at Trp43 mimics the defect of the proline-hinge mutants on closure *in vitro* and *in vivo*[28]. Therefore, closure and formation of the composite active site may couple decapping to stimulation by coactivators.

Our results are consistent with a model of decapping by Dcp2, in which the catalytic step consists of at least two substeps, beginning with isomerization to the active form (**Fig. 5b**) followed by the chemical step[39] (**Fig. 5c** and **Supplementary Note**). In the open form, the active site is incomplete, resulting in inefficient decapping (**Fig. 5b** and **Supplementary Fig. 1a**). Cap recognition by both domains induces closure and forms a composite active site, allowing for efficient decapping (**Fig. 5c**). Previous experiments revealed that 5′-monophosphate product RNA and nonhydrolyzable substrate RNA bind with the same affinity, suggesting cap recognition and closure occur after binding[27]. Dcp1 may accelerate the catalytic step by stabilizing the composite active site or enhancing the rate of closure. Like Dcp1, coactivators of decapping such as the Edc proteins in yeast[40,41], the NMD factors Upf2 and Upf3 (ref. 33), the heptameric Lsm1–Lsm7 complex[32], Pat1 (ref. 32) and others may stimulate decapping by altering this conformational equilibrium. This is similar to regulation of DEAD-box helicases by cofactors that couple conformational changes to ATP hydrolysis using a bipartite active site[42,43]. The scavenger decapping enzyme DcpS also uses a composite active site to decap 3′-to-5′ exosomal decay products but is different in fold, chemistry and regulation[44,45]. For Dcp2, coactivators have a critical role in regulation, and the new understanding of the active form presented here motivates further mechanistic studies to determine how regulation is achieved in different 5′-to-3′ mRNA decay pathways.

METHODS

Methods and any associated references are available in the online version of the paper at http://www.nature.com/nsmb/.

Note: Supplementary information is available on the Nature Structural & Molecular Biology website.

ACKNOWLEDGMENTS

We thank M. Kelly for NMR support; K. Krukenberg as well as beamline scientists G. Hura and M. Hammel of Beamline 12.3.1 at the Advanced Light Source for assistance with SAXS experimentation and data analysis; and J.J. Miranda, M. Pufall, G. Narlikar and D. Morgan for critical reading of the manuscript. This work was supported by US National Institutes of Health grant R01GM078360 to J.D.G. S.N.F. received support from the Sandler Family Foundation for Basic Sciences and the Achievement Awards for College Scientists Foundation. B.N.J. was supported by a National Science Foundation predoctoral fellowship. G.A.H. was a student in the University of California, San Francisco Summer Research Training Program. The Advanced Light Source is supported by US Department of Energy Contract No. DE-AC02-05CH11231.

AUTHOR CONTRIBUTIONS
S.N.F. designed and performed experiments, analyzed data, wrote the manuscript and prepared the figures; B.N.J. performed an experiment; G.A.H. generated Dcp2 mutants; J.D.G. supervised the project and experimental design and guided manuscript preparation.

COMPETING FINANCIAL INTERESTS
The authors declare no competing financial interests.

Published online at http://www.nature.com/nsmb/.
Reprints and permissions information is available online at http://npg.nature.com/reprintsandpermissions/.

1. Schier, A.F. The maternal-zygotic transition: death and birth of RNAs. *Science* **316**, 406–407 (2007).
2. Lindstein, T., June, C.H., Ledbetter, J.A., Stella, G. & Thompson, C.B. Regulation of lymphokine messenger RNA stability by a surface-mediated T cell activation pathway. *Science* **244**, 339–343 (1989).
3. Shyu, A.B., Greenberg, M.E. & Belasco, J.G. The c-fos transcript is targeted for rapid decay by two distinct mRNA degradation pathways. *Genes Dev.* **3**, 60–72 (1989).
4. Shaw, G. & Kamen, R. A conserved AU sequence from the 3′ untranslated region of GM-CSF mRNA mediates selective mRNA degradation. *Cell* **46**, 659–667 (1986).
5. Hilgers, V., Teixeira, D. & Parker, R. Translation-independent inhibition of mRNA deadenylation during stress in *Saccharomyces cerevisiae*. *RNA* **12**, 1835–1845 (2006).
6. Chowdhury, D. & Novina, C.D. RNAi and RNA-based regulation of immune system function. *Adv. Immunol.* **88**, 267–292 (2005).
7. Isken, O. & Maquat, L.E. Quality control of eukaryotic mRNA: safeguarding cells from abnormal mRNA function. *Genes Dev.* **21**, 1833–1856 (2007).
8. Wang, Z., Jiao, X., Carr-Schmid, A. & Kiledjian, M. The hDcp2 protein is a mammalian mRNA decapping enzyme. *Proc. Natl. Acad. Sci. USA* **99**, 12663–12668 (2002).
9. Beelman, C.A. *et al.* An essential component of the decapping enzyme required for normal rates of mRNA turnover. *Nature* **382**, 642–646 (1996).
10. Fenger-Grøn, M., Fillman, C., Norrild, B. & Lykke-Andersen, J. Multiple processing body factors and the ARE binding protein TTP activate mRNA decapping. *Mol. Cell* **20**, 905–915 (2005).
11. Chen, C.Y. & Shyu, A.B. AU-rich elements: characterization and importance in mRNA degradation. *Trends Biochem. Sci.* **20**, 465–470 (1995).
12. Amrani, N., Sachs, M.S. & Jacobson, A. Early nonsense: mRNA decay solves a translational problem. *Nat. Rev. Mol. Cell Biol.* **7**, 415–425 (2006).
13. Chen, C.Y., Zheng, D., Xia, Z. & Shyu, A. Ago-TNRC6 triggers microRNA-mediated decay by promoting two deadenylation steps. *Nat. Struct. Mol. Biol.* **16**, 1160–1166 (2009).
14. Eulalio, A. *et al.* Target-specific requirements for enhancers of decapping in miRNA-mediated gene silencing. *Genes Dev.* **21**, 2558–2570 (2007).
15. Behm-Ansmant, I. *et al.* mRNA degradation by miRNAs and GW182 requires both CCR4:NOT deadenylase and DCP1:DCP2 decapping complexes. *Genes Dev.* **20**, 1885–1898 (2006).
16. Rissland, O.S. & Norbury, C. Decapping is preceded by 3′ uridylation in a novel pathway of bulk mRNA turnover. *Nat. Struct. Mol. Biol.* **16**, 616–623 (2009).
17. Heo, I. *et al.* TUT4 in concert with Lin28 suppresses microRNA biogenesis through pre-microRNA uridylation. *Cell* **138**, 696–708 (2009).
18. Song, M.-G. & Kiledjian, M. 3′ terminal oligo U-tract-mediated stimulation of decapping. *RNA* **13**, 2356–2365 (2007).
19. Shen, B. & Goodman, H.M. Uridine addition after microRNA-directed cleavage. *Science* **306**, 997 (2004).
20. Stevens, A. & Maupin, M.K. A 5′—3′ exoribonuclease of *Saccharomyces cerevisiae*: size and novel substrate specificity. *Arch. Biochem. Biophys.* **252**, 339–347 (1987).
21. Coller, J. & Parker, R. Eukaryotic mRNA decapping. *Annu. Rev. Biochem.* **73**, 861–890 (2004).
22. Franks, T.M. & Lykke-Andersen, J. The control of mRNA decapping and p-body formation. *Mol. Cell* **32**, 605–615 (2008).
23. Garneau, N.L., Wilusz, J. & Wilusz, C.J. The highways and byways of mRNA decay. *Nat. Rev. Mol. Cell Biol.* **8**, 113–126 (2007).
24. Krogan, N.J. *et al.* Global landscape of protein complexes in the yeast *Saccharomyces cerevisiae*. *Nature* **440**, 637–643 (2006).
25. Parker, R. & Sheth, U. P bodies and the control of mRNA translation and degradation. *Mol. Cell* **25**, 635–646 (2007).
26. She, M. *et al.* Structural basis of dcp2 recognition and activation by dcp1. *Mol. Cell* **29**, 337–349 (2008).
27. Deshmukh, M.V. *et al.* mRNA decapping is promoted by an RNA-binding channel in Dcp2. *Mol. Cell* **29**, 324–336 (2008).
28. She, M. *et al.* Crystal structure and functional analysis of Dcp2p from *Schizosaccharomyces pombe*. *Nat. Struct. Mol. Biol.* **13**, 63–70 (2006).
29. Mildvan, A.S. *et al.* Structures and mechanisms of Nudix hydrolases. *Arch. Biochem. Biophys.* **433**, 129–143 (2005).
30. Bessman, M.J., Frick, D.N. & O'Handley, S.F. The MutT proteins or "Nudix" hydrolases, a family of versatile, widely distributed, "housecleaning" enzymes. *J. Biol. Chem.* **271**, 25059–25062 (1996).
31. Piccirillo, C., Khanna, R. & Kiledjian, M. Functional characterization of the mammalian mRNA decapping enzyme hDcp2. *RNA* **9**, 1138–1147 (2003).
32. Teixeira, D. & Parker, R. Analysis of P-body assembly in *Saccharomyces cerevisiae*. *Mol. Biol. Cell* **18**, 2274–2287 (2007).
33. Sheth, U. & Parker, R. Targeting of aberrant mRNAs to cytoplasmic processing bodies. *Cell* **125**, 1095–1109 (2006).
34. Sheth, U. & Parker, R. Decapping and decay of messenger RNA occur in cytoplasmic processing bodies. *Science* **300**, 805–808 (2003).
35. Jones, B.N., Quang-Dang, D.-U., Oku, Y. & Gross, J.D. A kinetic assay to monitor RNA decapping under single-turnover conditions. *Methods Enzymol.* **448**, 23–40 (2008).
36. Gabelli, S.B., Bianchet, M.A., Bessman, M.J. & Amzel, L.M. The structure of ADP-ribose pyrophosphatase reveals the structural basis for the versatility of the Nudix family. *Nat. Struct. Biol.* **8**, 467–472 (2001).
37. Kalodimos, C.G. *et al.* Structure and flexibility adaptation in nonspecific and specific protein-DNA complexes. *Science* **305**, 386–389 (2004).
38. von Hippel, P.H. & Berg, O.G. Facilitated target location in biological systems. *J. Biol. Chem.* **264**, 675–678 (1989).
39. Floor, S., Jones, B. & Gross, J. Control of mRNA decapping by Dcp2: an open and shut case? *RNA Biol.* **5**, 189–192 (2008).
40. Dunckley, T., Tucker, M. & Parker, R. Two related proteins, Edc1p and Edc2p, stimulate mRNA decapping in *Saccharomyces cerevisiae*. *Genetics* **157**, 27–37 (2001).
41. Decker, C.J., Teixeira, D. & Parker, R. Edc3p and a glutamine/asparagine-rich domain of Lsm4p function in processing body assembly in *Saccharomyces cerevisiae*. *J. Cell Biol.* **179**, 437–449 (2007).
42. Schutz, P. *et al.* Crystal structure of the yeast eIF4A-eIF4G complex: An RNA-helicase controlled by protein-protein interactions. *Proc. Natl. Acad. Sci. USA* **105**, 9564–9569 (2008).
43. Caruthers, J.M. & McKay, D.B. Helicase structure and mechanism. *Curr. Opin. Struct. Biol.* **12**, 123–133 (2002).
44. Gu, M. *et al.* Insights into the structure, mechanism, and regulation of scavenger mRNA decapping activity. *Mol. Cell* **14**, 67–80 (2004).
45. Wang, Z. & Kiledjian, M. Functional link between the mammalian exosome and mRNA decapping. *Cell* **107**, 751–762 (2001).
46. Mori, S., Abeygunawardana, C., Johnson, M.O. & van Zijl, P.C. Improved sensitivity of HSQC spectra of exchanging protons at short interscan delays using a new fast HSQC (FHSQC) detection scheme that avoids water saturation. *J. Magn. Reson. B.* **108**, 94–98 (1995).

ONLINE METHODS

Protein purification, mutagenesis and decapping complex formation. *S. pombe* $Dcp2_{1–243}$ and *S. pombe* $Dcp1_{1–127}$ were PCR-amplified from *S. pombe* cDNA and cloned into p-His-GB1-parallel[47]. The catalytic domain (95–243) was PCR-amplified from *S. pombe* $Dcp2_{1–243}$ and cloned into p-His-GB1-parallel, and the regulatory domain (1–94) was PCR-amplified from *S. pombe* $Dcp2_{1–243}$ and cloned into a vector derived from pet28a consisting of a histidine tag, Tobacco Etch Virus (TEV) protease site and a multiple cloning site (His-TEV-$Dcp2_{1–94}$). All proteins were expressed independently in *E. coli*. Cells were lysed by sonication and clarified by centrifugation at 16,000*g*, and then overexpressed proteins were purified using nickel-nitrilotriacetic acid affinity chromatography. Elutions were digested with TEV protease and then subjected to a second nickel-affinity column to remove the His-GB1 tag. The second nickel purification was not used in purification of $Dcp2_{1–94}$ because the histidine tag is easily resolved by gel filtration. The Dcp1–Dcp2 complex was formed following TEV protease cleavage by incubation of 1.1:1 Dcp1:Dcp2 molar ratio for 4 h at 4 °C before gel filtration. All mutants were made using whole plasmid PCR with mutagenic divergent primers; sequences of the Dcp2 ORF were confirmed by dideoxy sequencing.

NMR spectroscopy. Proteins were purified as above and subjected to gel-filtration chromatography using a Superdex G75 column in 200 mM NaCl, 100 mM Na_2SO_4, 5 mM DTT, 21.1 mM NaH_2PO_4 and 28.8 mM Na_2HPO_4 (pH 7.0) for storage and backbone resonance assignment. Prior to nucleotide titrations, proteins were exchanged into 150 mM NaCl, 2 mM $MgCl_2$, 5 mM DTT and 50 mM HEPES (pH 7.0) using a desalting column (BioRad). Titrations on the regulatory domain were performed at 100 µM protein in a volume of 500 µl by simultaneous addition of equimolar nucleotide and magnesium. Titrations on the catalytic domain were identical except that they were performed in the absence of magnesium. All titration experiments were conducted on a Bruker Avance 800 MHz spectrometer outfitted with a cryogenic probe. Titration data were only fitted if the change in chemical shift between apo and 30 mM nucleotide for a given residue was greater than the mean plus one s.d. Assignments were obtained from standard triple-resonance experiments[48] (HNCA, HNCOCA, HNCO, HNCACO, HNCACB and HNCOCACB) on a Varian 600 MHz spectrometer, with additional verification from a ^{15}N-dispersed NOESY on a Bruker Avance 800 MHz spectrometer. All assignment experiments were performed using cryogenic probes at 500 µM protein. Assignments were obtained for 88 of 94 residues in $Dcp2_{1–94}$ (the regulatory domain) and for 104 of 148 residues in $Dcp2_{95–243}$ (the catalytic domain). In $Dcp2_{95–243}$, the majority (30 of 44) of the unassigned residues were in a loop (from 194–224) that is not visible in the nitrogen HSQC.

Small-angle X-ray scattering. Samples were purified as described and subjected to gel-filtration chromotography using a Superdex G75 column in 150 mM NaCl, 2 mM DTT and 50 mM HEPES pH 7.0. All SAXS experiments were performed on stoichiometric Dcp1–Dcp2 complex with mutations in Dcp2 as indicated. Raw data was processed via scripts provided by ALS Beamline 12.3.1 scientists[49], and buffer was subtracted. In some cases, buffer subtraction was performed manually by reweighting the normalization of the protein scattering to the buffer scattering because there were small differences in nucleotide concentration between protein and buffer blank. This manual subtraction did not affect the distance distribution function and was used to achieve an intensity curve that asymptotes to zero at high values of momentum transfer. In no case was this correction larger than 5%. Following raw data processing, distance distribution functions were computed using GNOM[50]. D_{max} was explored between 80 and 150 Å in increments of 5 Å, and the smallest value that led to a monotonic decrease toward $P(D_{max}) = 0$ was selected. $P(D_{max}) = 0$ was then enforced via GNOM. Notably, the D_{max} parameter is simply an integration limit for the indirect Fourier transform method of calculating the distance distribution function and is not necessarily a measure of the maximum particle dimension, as it is highly sensitive to aggregation[50–52].

Decapping assays. Proteins were purified as described and subjected to gel-filtration chromatography using a Superdex G75 column in buffer containing 100 mM NaCl, 5% (v/v) glycerol, 5 mM DTT and 50 mM HEPES (pH 7.5). Proteins were prepared for kinetics as described[35]. Rates were measured at a series of enzyme concentrations on a 29-mer substrate[27] in an ice block at ~0.1 °C. Rates for each enzyme concentration were calculated by dividing the initial rate during the linear phase of the reaction by the endpoint of 0.85. Each assay was repeated at least twice, and the rate for each enzyme concentration was averaged between experiments. These average rates were then plotted versus concentration, with error bars representing the s.e.m. between independent experiments. Data were fitted to extract K_M and k_{max} as described[35].

Solvent accessibility calculations. The SASA[53] for the regulatory domain was calculated using the program areaimol within the CCP4 suite[54]. The open and closed SASA values were calculated using the open or closed crystal structures, respectively (PDB 2QKM[26]). The SASA for each residue was normalized to 75% of the maximum value calculated from a Gly-X-Gly tripeptide[55]. The factor of 75% was introduced because the helical 31–52 region is less exposed than a Gly-X-Gly tripeptide, and the largest observed SASA was close to 75% of the Gly-X-Gly value (residue 33).

Multiple sequence alignments. Sequences for Dcp2 from 10 organisms were retrieved from the National Center for Biotechnology Information database, aligned using MUSCLE[56] and visualized using Jalview[57]. Shown in **Figure 1** is a fragment of an alignment that was carried out using default MUSCLE parameters on the entire sequence of Dcp2. The species used for the alignment were *S. pombe*, *S. cerevisiae*, *Candida albicans*, *Arabidopsis thaliana*, *Caenorhabditis elegans*, *Drosophila melanogaster*, *Xenopus laevis*, *Danio rerio*, *Mus musculus* and *Homo sapiens*, with eight of these shown.

47. Card, P.B. & Gardner, K.H. Identification and optimization of protein domains for NMR studies. *Methods Enzymol.* **394**, 3–16 (2005).
48. Ferentz, A.E. & Wagner, G. NMR spectroscopy: a multifaceted approach to macromolecular structure. *Q. Rev. Biophys.* **33**, 29–65 (2000).
49. Hura, G.L. *et al.* Robust, high-throughput solution structural analyses by small angle X-ray scattering (SAXS). *Nat. Methods* **6**, 606 (2009).
50. Svergun, D.I. Determination of the regularization parameter in indirect-transform methods using perceptual criteria. *J. Appl. Crystallogr.* **25**, 495–503 (1992).
51. Putnam, C.D., Hammel, M., Hura, G.L. & Tainer, J.A. X-ray solution scattering (SAXS) combined with crystallography and computation: defining accurate macromolecular structures, conformations and assemblies in solution. *Q. Rev. Biophys.* **40**, 191–285 (2007).
52. Glatter, O. & Kratky, O. *Small Angle X-ray Scattering* (Academic Press, London, 1982).
53. Lee, B. & Richards, F.M. The interpretation of protein structures: estimation of static accessibility. *J. Mol. Biol.* **55**, 379–400 (1971).
54. Collaborative Computational Project. N. The CCP4 suite: programs for protein crystallography. *Acta Crystallogr. D Biol. Crystallogr.* **50**, 760–763 (1994).
55. Chothia, C. The nature of the accessible and buried surfaces in proteins. *J. Mol. Biol.* **105**, 1–12 (1976).
56. Edgar, R.C. MUSCLE: multiple sequence alignment with high accuracy and high throughput. *Nucleic Acids Res.* **32**, 1792–1797 (2004).
57. Waterhouse, A.M., Procter, J.B., Martin, D.M.A., Clamp, M. & Barton, G.J. Jalview Version 2–a multiple sequence alignment editor and analysis workbench. *Bioinformatics* **25**, 1189–1191 (2009).

doi:10.1038/nsmb.1879